

Inverse problems: Can we obtain more? Quantum dynamics and the ${}^4\text{He}$ case

E. Vitali, M. Rossi, L. Reatto, and D.E. Galli

Dipartimento di Fisica, Università degli Studi di Milano, via Celoria 16, 20133 Milano, Italy

(Dated: March 9, 2019)

We introduce a new strategy, called Genetic Inversion via Falsification of Theories (GIFT), to face inverse problems and we apply it to the extraction of information about real time dynamics of a many-body quantum system from noisy imaginary time correlation functions $f(\tau)$ computed via Quantum Monte Carlo (QMC). Production and falsification of model spectral functions $s(\omega)$ are obtained via a survival-to-compatibility with $f(\tau)$ evolutionary process, based on Genetic Algorithms. Statistical uncertainty in $f(\tau)$ is promoted to be an asset via a sampling of equivalent $f(\tau)$ within the noise, which give rise to independent evolutionary processes. We have studied bulk ${}^4\text{He}$ at $T = 0$ K; for the first time we recover from exact QMC simulations sharp quasi-particle excitations with spectral functions displaying also the multiphonon branch. As further applications of the method we have studied the impuriton branch of one ${}^3\text{He}$ atom in liquid ${}^4\text{He}$ and the vacancy-wave excitations in hcp solid ${}^4\text{He}$ finding a novel roton like feature.

PACS numbers: 02.30.Zz; 67.40.Db; 67.55.Jd; 67.55.Lf; 67.80.-s

I. INTRODUCTION

Since the earliest days of research in Physics, *inverse problems* have always provided challenges in a huge variety of physical or even more generally scientific studies^{1,2}. At the most general level, an inverse problem consists in using experimental *observations* in order to infer the values of the parameters of a *theory* describing a natural phenomenon. At a first glance, one immediately convinces himself that such an inverse procedure in most realistic situations is unavoidably ill-posed, since any set of observations is limited and noisy, thus ruling out the possibility of finding out one and only one theory whose predictions fit such data. In more abstract terms, the problem of inverting a map connecting a *space of theories*, say \mathcal{S} , and a *space of data*, say \mathcal{D} , is mathematically ill-posed; the reason for this lies in the inescapable limitations related to any realistic way of performing observations, making impossible to have access to a sufficiently exhaustive and accurate knowledge of the space \mathcal{D} .

Some important questions thus naturally arise: what can we really learn when facing an inverse problem? What do we mean when we speak about a *solution*? In our opinion, a key proposition is brilliantly put forward in Ref.3, following Popper⁴: observations may be used only to *falsify* a theory. In other words, we cannot expect to find out a recipe that will allow to *deduce* all what is needed to build up a unique theory from a given set of observed data. Nevertheless, provided that we are able to construct a suitable parametrization of the abstract space of theories \mathcal{S} , we may use observations to provide a “falsification test”, aimed to exclude the theories whose predictions fail to fit the data. In this way we will be able to collect a (maybe very big) class of theories, which have been not falsified by the measured data. In our opinion, the best way to achieve this is to fully exploit all the information related to the observations: that is, since any set of experimental data appears together with statistical uncertainties evaluated starting

from suitable measurements, *any* set of data compatible with the original one has to take part to the falsification test, in order to suppress the possibility of unphysical effects arising from statistical fluctuations.

Once we remain with a set of equivalent “solutions” “survived” to the falsification test, depending on the mathematical details of the space \mathcal{S} , a natural idea appears to be that of devising a procedure allowing to capture what do the “survived” theories have in common. In this way, even if we won’t succeed in finding out a unique theory $s \in \mathcal{S}$, we will be able nevertheless to find out a class of features, providing physical properties, that s has to possess so that it will not be falsified by the limited set of observations.

A. Inverse problems and quantum dynamics

In the last decades new ways of performing “*observations*”, computer simulations, have emerged in many areas of scientific research and have provided new sources of inverse problems. In this work we focus on one in particular, and namely on the estimation of spectral functions of many-body quantum systems starting from imaginary time correlation functions computed in Quantum Monte Carlo (QMC) simulations. Indeed, the study of dynamical properties requires the evaluation of spectral functions $s(\omega)$:

$$s(\omega) = \int_{-\infty}^{+\infty} \frac{dt}{2\pi} e^{i\omega t} \langle e^{i\hat{H}t} \hat{A} e^{-i\hat{H}t} \hat{B} \rangle, \quad (1)$$

\hat{A} and \hat{B} being given operators acting on the Hilbert space of the system whose Hamiltonian operator is \hat{H} . The brackets indicate expectation value on the ground state or thermal average. Unfortunately, general methods to obtain exact real time evolution are not known, thus forcing us to *deduce* a *theoretical* $s(\omega)$ from “*observations*” of imaginary time correlation function $f(\tau) =$

$\langle e^{\hat{H}\tau} \hat{A} e^{-\hat{H}\tau} \hat{B} \rangle$ which can be computed by QMC methods. The scenario is that of an inverse problem with the formal appearance of an integral equation

$$f(\tau) = \int_{-\infty}^{+\infty} d\omega \mathcal{K}(\tau, \omega) s(\omega) \quad (2)$$

where for example, at zero temperature, $\mathcal{K}(\tau, \omega) = \theta(\omega) e^{-\tau\omega}$, $\theta(\omega)$ being the Heaviside distribution. The difficulty lies in the fact that the kernel $\mathcal{K}(\tau, \omega)$ is a smoothing operator and QMC techniques are based on a discretization of the imaginary time domain, with time step $\delta\tau$, allowing an estimation of $f(\tau)$ only in correspondence with a finite number of imaginary time values $\{0, \delta\tau, 2\delta\tau, \dots, l\delta\tau\}$,

$$\mathcal{F} \equiv \{f_0, f_1, \dots, f_l\}. \quad (3)$$

In general \mathcal{F} is obtained as an average of several QMC calculations of $f(\tau)$, each affected by statistical noise and which are used to estimate the *statistical uncertainties* $\{\sigma_{f_0}, \sigma_{f_1}, \dots, \sigma_{f_l}\}$ associated with \mathcal{F} . The task is then to evaluate $s(\omega)$ starting from limited and noisy data. Often sum rules provide useful help, either imposing exact constraints on $s(\omega)$ or allowing to perform additional QMC measurements which provide estimations for some moments of $s(\omega)$:

$$\mathcal{C} \equiv \{c_n = \int_{-\infty}^{+\infty} d\omega \omega^n s(\omega), n \in \mathbb{Z}\}. \quad (4)$$

For example $c_0 = \langle \hat{A} \hat{B} \rangle$ may be easily estimated in equilibrium QMC simulations with an associated statistical uncertainty. Moreover some *a priori knowledge* may be assumed such as the support, non-negativity or some further properties.

The task of facing the problem in equation (2), namely an analytic continuation problem, has already been investigated: the Maximum Entropy Method⁵ (MEM) is the most widely popular strategy developed; in the realm of bulk quantum fluids it has provided only qualitatively interesting results^{6,7}. Another method has been proposed, the Average Spectrum Method⁸ (ASM), which has been recently applied to lattice spin models⁹ but also to realistic off-lattice systems¹⁰. The ASM strategy captures the idea of extracting physical properties using only observations. Here we want to insist on this idea, introducing a new way to deal with the observations and their uncertainties strongly inspired by the falsification principle. As explained below, to do this we need a space of models \mathcal{S} , containing a wide collection of spectral functions consistent with any *prior knowledge* about $s(\omega)$, a falsification procedure relying on the QMC “measurements” $\mathcal{D} = \{\mathcal{F}, \mathcal{C}\}$ and a strategy to capture the accessible physical properties of $s(\omega)$. The strategy we are going to describe in the following relies on Genetic Algorithms¹² to explore \mathcal{S} and falsify its elements; for this reason we have called it the Genetic Inversion via Falsification of Theories (GIFT) method. A preliminary application of this

strategy to the determination of the dynamical structure factor $S(q, \omega)$ of liquid ⁴He was presented in Ref.13; here we explain in detail the GIFT method and we present several applications to the Helium system.

The structure of the paper is the following. In section II we introduce the genetic inversion strategy; in section III we show applications of the GIFT method on several Helium systems; in section IV we present tests on the reliability of the GIFT method on known spectral models; section V contains our conclusions.

II. GENETIC INVERSION STRATEGY

A. The space of models

In our mathematical framework \mathcal{S} contains a wide class of step functions, providing a compromise between the possibility of suitably approximating *any* model of spectral function and the feasibility of numerical operations inside it. In the typical case ($\hat{A} = \hat{B}^\dagger$) when $s(\omega)$ is known to be real-valued, non-negative and the zero-moment sum-rule holds, we rely on models \bar{s} of the form:

$$\bar{s}(\omega) = \sum_{j=0}^{N_\omega-1} \frac{s_j}{\mathcal{M}\Delta\omega} \chi_{A_j}(\omega), \quad \sum_{j=0}^{N_\omega-1} s_j = \mathcal{M} \quad . \quad (5)$$

$\bar{s}(\omega)$ differs from the physical spectral functions by a factor c_0 , the zero-moment sum rule, which belongs to the set of observations and its role will become evident below. We introduce a discretization of the codomain:

$$s_j \in \mathbb{N} \cup \{0\}, \quad (6)$$

to make the space finite, and we use the characteristic function $\chi_{A_j}(\omega)$ of the intervals $A_j = [\omega_j, \omega_{j+1})$, $\{\omega_0, \dots, \omega_{N_\omega}\}$ being a partition of width $\Delta\omega$ of an interval of the real line larger than the hypothesized support of $s(\omega)$. \mathcal{M} provides the maximum number of quanta of spectral weight available for the ensemble of the intervals A_j .

B. The falsification principle

Once we have defined the space of model spectral functions, we have to devise a practical strategy to implement the falsification principle. We have to rely on the QMC estimations of the imaginary time correlation functions (and, in general, also of the moments):

$$\mathcal{F} \equiv \{f_0, f_1, \dots, f_l\}. \quad (7)$$

Such numbers are averages evaluated during a simulation and appear together with their estimated statistical uncertainties $\{\sigma_{f_0}, \sigma_{f_1}, \dots, \sigma_{f_l}\}$. In typical approaches, such information are dealt with inside the framework

of Bayes' theorem; they provide the key ingredients to build up the *a posteriori* probability⁵ to be maximized, together with some *a priori* probability, to extract the *most probable* spectral function.

On the other hand, we find natural to suggest a new way of exploiting the information contained in $\{\sigma_{f_0}, \sigma_{f_1}, \dots, \sigma_{f_l}\}$: any set \mathcal{F}^* *equivalent* to (7), i.e. such that $|f_i^* - f_i|$ is of the same order as σ_{f_i} , could be a result of another hypothetical simulation. Falsifying the elements of \mathcal{S} should require not only compatibility with \mathcal{F} but also compatibility with a vast population of \mathcal{F}^* equivalent to the set (7) of data. At a practical level our aim is twofold: on one hand we need a recipe to generate *equivalent* sets \mathcal{F}^* , on the other hand we have to use the generated \mathcal{F}^* to falsify the elements of \mathcal{S} . At the simplest level we have addressed the generation of the sets \mathcal{F}^* by sampling independent Gaussian distributions centered on the original observations, with variances which correspond to the estimated statistical uncertainties so that a generic element \mathcal{F}^* is:

$$\mathcal{F}^* \equiv \{f_0 + \varepsilon_0^*, f_1 + \varepsilon_1^*, \dots, f_l + \varepsilon_l^*\} = \{f_0^*, f_1^*, \dots, f_l^*\} \quad (8)$$

being ε_j^* random numbers sampled from Gaussian distributions with zero mean and variances equal to $\sigma_{f_j}^2$. We stress that the very idea of exploiting the statistical uncertainties in the observations for generating *equivalent* sets \mathcal{F}^* is the main difference with respect to preexisting statistical approaches to inverse problems. Note that in presence of more complete information in the observations, like an estimation of the full covariance matrix, Σ , the generation of the equivalent sets \mathcal{F}^* can be readily generalized by sampling an $(l+1)$ -variate normal distribution with the following probability density function:

$$p(\mathcal{F}^*) = \frac{\exp\left[-\frac{1}{2}(\mathcal{F}^* - \mathcal{F})^\top \Sigma^{-1}(\mathcal{F}^* - \mathcal{F})\right]}{(2\pi)^{\frac{l+1}{2}} \det(\Sigma)^{\frac{1}{2}}} \quad ; \quad (9)$$

standard methods to perform efficiently this task are known (see for example Ref.11). To be precise, being the set \mathcal{F} a QMC estimation of the (unknowable) exact correlation function values, the probability density function $p(\mathcal{F}^*)$ in the previous equation does not represent the (unknowable) exact distribution of the observations; this situation is typical of the inverse problems we are considering and of the statistical methods developed in this context: we have to rely on what we have observed. Therefore, it is important to estimate the statistical uncertainties connected with the application of a particular statistical method. This can always be obtained comparing models coming from the analysis of independent observations.

The key point is then to falsify the elements of \mathcal{S} relying on each one of these sets: compatibility means small deviations from the observations. Thus, given the set \mathcal{F}^* , a very simple measure of the compatibility of a model with this set of observations can be obtained by comput-

ing

$$\Delta(\bar{s}) = \frac{1}{l+1} \sum_{j=0}^l \left[f_j^* - \int d\omega e^{-\omega j \delta \tau} c_0^* \bar{s}(\omega) \right]^2 \quad . \quad (10)$$

The normalization of our models requires the multiplication of $\bar{s}(\omega)$ by c_0 , the zero moment, which however belongs to the set of observations; a natural choice is to sample also its value analogously to how we treat \mathcal{F} . This is the reason why a factor c_0^* appears in (10). Each member \mathcal{F}^* of equivalent data leads to a different model; let us call \bar{s}_k the model found with the k -th member \mathcal{F}^* . Each one of these models cannot be trusted to be the solution of the inverse problem, being at least partially biased by the particular \mathcal{F}^* ; in other terms we can say that each one of these models will possess spurious information, presumably different in each model, together with some physical information. An averaging procedure is therefore the simplest way to filter out the spurious information and to reveal physical information, which consist in the common features among the models which have not been falsified. Therefore we take as the reconstructed spectral function the average

$$S_{GIFT}(\omega) = \frac{1}{\mathcal{N}_r} \sum_{k=1}^{\mathcal{N}_r} c_0^{(k)} \bar{s}_k(\omega) \quad (11)$$

where \mathcal{N}_r is the number of equivalent random set of \mathcal{F}^* used in the computation and $c_0^{(k)}$ is the c_0^* used in the k -th reconstruction.

The average procedure in the definition of $S_{GIFT}(\omega)$ points toward some similarities between our strategy and that of ASM. However, in the light of the falsification principle, the two methods are fairly different: in order to obtain its "solution", ASM averages over spectral functions obtained by exploring model-space regions via a local Metropolis random walk based on a probability distribution;⁸ thus ASM regards all the sampled spectral functions, also those with a low probability (of course, they are rarely sampled) as models which have not been falsified. Moreover, with ASM the statistical uncertainties in the observations play a different role, appearing only in the definition of the probability. Another issue is the algorithm used to explore the space of models; as explained below, GIFT uses a *non-local* dynamics induced by a stochastic evolutionary process instead of a local Metropolis random walk which, in principle, could suffer from ergodicity problems, being the high probability model-space regions not guaranteed to be simply connected. Which of the two approaches, GIFT and ASM is superior might well depend on the specific inverse problem or, in practice, it is possible that the reconstruction abilities of GIFT and ASM are essentially equivalent. ASM has never been applied to the ⁴He case, it will be interesting in the future to compare the two methods on the same inverse problem.

The natural scale of $\Delta(\bar{s})$ is provided by the value $\delta = \frac{1}{l+1} \sum_{j=0}^l \sigma_{f_j}^2$: models \bar{s} such that $\Delta(\bar{s}) \ll \delta$

may provide unphysical overfitting. In our statistical approach to inverse problems there are two procedures which preserve from overfitting. The first one is that, given a set \mathcal{F}^* , the exploration of the space of models \mathcal{S} should be stopped when a model $\bar{s}(\omega)$ is found such that $\Delta(\bar{s}) \simeq \delta$; a further reduction of Δ will only represent the intention to give to \mathcal{F}^* a strong belief, which is incompatible with the statistical treatment of the observations in our strategy. The second procedure is even more relevant and in some sense it is intrinsic to our strategy: given an \mathcal{F}^* the reconstructed model $\bar{s}(\omega)$ contains some spurious information, but these information will be averaged out in $S_{GIFT}(\omega)$.

At this point the following question urges an answer: How can we practically explore \mathcal{S} ? We want to stress that the answer to this question is not the key point of our strategy; as we explain in the following, we have implemented genetic algorithms as efficient algorithms to explore our huge space of models, \mathcal{S} . There could be inverse problems and different space of models which could be more efficiently explored with other algorithms; obviously, our strategy, which consists mainly in the new statistical treatment of observations, can be applied also in these cases.

C. The fitness and the genetic dynamics

Genetic algorithms (GA) provide an extremely efficient tool to explore a sample space by a *non-local* stochastic dynamics, via a survival-to-fitness evolutionary process mimicking the natural selection we observe in natural world; such evolution aims toward “good” *building blocks*¹² which, in our case, should recover information on physical spectral functions. The fitness of one particular $\bar{s}(\omega)$ should be based on the observations, i.e., on the noisy measured set $\mathcal{D} = \{\mathcal{F}, \mathcal{C}\}$. But as explained before, taking into account the estimated statistical noise of \mathcal{D} , any set \mathcal{D}^* compatible with \mathcal{D} provides equivalent information to build a fitness function. Thus in our GA any random set $\mathcal{D}^* = \{\mathcal{F}^*, \mathcal{C}^*\}$ ¹⁴ gives rise to a fitness, which simply compares “predictions” of theories and “observations”:

$$\Phi_{\mathcal{D}^*}(\bar{s}) = -\Delta(\bar{s}) - \sum_n \gamma_n \left[c_n^* - \int d\omega \omega^n c_0^* \bar{s}(\omega) \right]^2 \quad (12)$$

In (12) the free parameters $\gamma_n > 0$ are adjusted in order to make the contributions to $\Phi_{\mathcal{D}^*}$ coming from \mathcal{F}^* and from \mathcal{C}^* of the same order of magnitude: the idea is that we are not allowed to prefer some particular observation among the others, thus they should have the same weight in the fitness. If it happens that one c_n is exactly known, no error is added making $c_n^* = c_n$. We stress that (12) provides the simplest and the most natural definition; moreover, as explained below, our GA uses $\Phi_{\mathcal{D}^*}$ only to order models in ascending fitness, thus any alternative definition of $\Phi_{\mathcal{D}^*}$ which provides the same ordering will give rise to an identical GIFT algorithm.

GA are well known procedures characterized by well defined (genetic-like) operations on populations of candidate solution to optimization problems in applied mathematics. For basic nomenclature and standard implementations one can refer to textbooks (e.g. see 12). Here we simply sketch our particular realization related to the space of models we have defined. In our GA, we start randomly constructing a collection of $\bar{s}(\omega)$; each $\bar{s}(\omega)$ is coded by N_ω integers, s_j in equation (5). The genetic dynamics then consists in a succession of *generations* during which an initial *population*, consisting of $\mathcal{N}_{\bar{s}}$ *individuals*, is replaced with new ones in order to reach regions of \mathcal{S} where high values of the *fitness* exist, for a given \mathcal{D}^* .

In practice, in the passage between two generations a succession of “biological-like” processes takes place, and namely *selection*, *crossover* and *mutation*. The *selection* procedure is meant to make individuals with large fitness preferentially be chosen to give rise to the next generation: we achieved this by ordering the population in ascending fitness and *selecting* the k -th individual with

$$k = \left[\mathcal{N}_{\bar{s}} r^{1/3} \right] + 1 \quad (13)$$

where r is a uniform random number, $r \in [0, 1)$, and $[\dots]$ is the integer part; the non linear dependence of k on r ensures that individuals with large fitness are preferentially selected. The *crossover* then operates on two selected $\bar{s}(\omega)$, the *father* and the *mother*, exchanging subparts of their total number of quanta of spectral weight, \mathcal{M} , to generate two *sons*. We have used a special single point crossover by sampling a random integer, w , between 0 and \mathcal{M} and by exchanging w randomly chosen quanta of spectral weight between the *father* and the *mother*. In this way, the second equation in (5) is automatically satisfied, implying that the zero-moment sum rule is also satisfied. Each exchanged quantum remains in the original frequency bin as in its parents, thus ensuring that strong features present in both parents tend to persist in the sons. Successively, with a given probability, *mutation* takes place on the two new individuals, i.e., a shift of a fraction of spectral weight between two intervals A_j . This is repeated till a new generation of $\bar{s}(\omega)$ replaces the old one, with the exception of the $\bar{s}(\omega)$ with the highest fitness in the old generation which is cloned (elitism). The number of individuals in the new population is constantly reduced by about 5% at every generation till $\mathcal{N}_{\bar{s}}$ is equal to a given minimal value; from this point over, the number of individuals $\mathcal{N}_{\bar{s}}$ in the new generations is kept constant to this minimum value. The discarded individuals are those with the smallest fitness in the population. This is done to start the genetic evolution from a wide variety of possible models, but to not dissipate computational time on falsified spectral functions.

In our context the GA dynamics performs the falsification procedure: only the $\bar{s}(\omega)$ with the highest fitness in the last generation provides a model, $\bar{s}_k(\omega)$, which has not been falsified by \mathcal{D}^* . The evolutionary process

stops either after a reasonable maximum amount of generations, $\mathcal{N}_{\mathcal{G}}$, or when a model $\bar{s}(\omega)$ is found such that $\Delta(\bar{s}(\omega)) \simeq \delta$. Many independent evolutionary processes are generated by sampling different \mathcal{D}^* , thus obtaining a set made of the elements $c_0^{(k)} \bar{s}_k(\omega)$; at this point, as explained above, an averaging procedure inside this set appears as the most natural way to extract physical information.

III. RESULTS FOR HELIUM SYSTEMS

We are ready now to present applications of our approach on physical systems. Long Monte Carlo runs have been performed in order to get imaginary time correlation functions with a typical statistical uncertainty of 0.1-1%. For bulk superfluid ^4He most of the simulations have been for $N = 64$ and $N = 256$ atoms moving in a cubic box, but also $N = 128$ and $N = 512$ have been studied; for solid ^4He the hcp lattice with $N = 180$ and $N = 448$ lattice position have been used. Imaginary time correlation functions have been computed for instants $\tau_l = l\delta\tau$, $l = 0, \dots, l_{max} = 60$ in the superfluid phase and $l_{max} = 30$ in the solid phase, spaced by $\delta\tau = 1/160 \text{ K}^{-1}$. In the present applications on ^4He systems the whole covariance matrix has not been computed, thus equivalent sets \mathcal{F}^* have been sampled simply by using the procedure in equation (8). We have tested on a very simple quantum system that the knowledge of the whole covariance matrix for the imaginary time correlation function does not improve the reconstruction abilities of our strategy¹⁶ when the kernel in equation (2) is of the form $\mathcal{K}(\tau, \omega) = \theta(\omega)e^{-\tau\omega}$; a similar conclusion was obtained in previous studies of superfluid ^4He via MEM.⁶ All the results shown in this article have been obtained with the interatomic interaction of Ref.17, but some computations have been performed also with that in Ref.18 as mentioned in the text. We have used the pair-product approximation¹⁹ to express the imaginary time propagator in the interval $\delta\tau = 1/160 \text{ K}^{-1}$ which is known to be very accurate. For bulk superfluid ^4He we chose $\gamma_n = 0 \forall n \neq 1$ (see equation (12)), i.e., we have included only c_0 , which is the static structure factor, and the first moment sum-rule which is exactly known, $c_1 = |\bar{q}|^2/2m$. For the extraction of the impurity branch and of the vacancy excitation spectrum we have only used the zero moment sum rule. Other parameters were fixed to $\Delta\omega = 0.25 \text{ K}$, $\mathcal{M} = 5000$, $N_\omega = 600 - 1600$, initial value of $\mathcal{N}_{\bar{s}} = 25000$ which is decreased down to the minimum value $\mathcal{N}_{\bar{s}} = 400$, as explained above; we have used about 10^3 different sets \mathcal{D}^* and the number of generations for a given \mathcal{D}^* have been fixed to 10^4 . We have performed many tests with different choices of such parameters showing that none has a critical role once $N_\omega\Delta\omega$ is larger of the support of the reconstructed spectral functions.

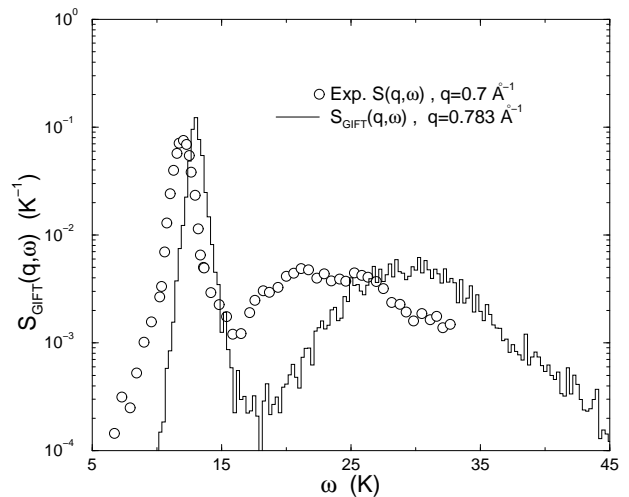


Figure 1: (line) $S_{GIFT}(q, \omega)$ for $q = 0.783 \text{ \AA}^{-1}$ and $\rho = 0.0218 \text{ \AA}^{-3}$; (open circles) observed¹⁵ dynamic structure factor $S(q, \omega)$ in liquid ^4He for $q = 0.7 \text{ \AA}^{-1}$ at SVP and $T = 1.3 \text{ K}$. Notice the logarithmic scale. Notice also the difference between the wave vector of $S_{GIFT}(q, \omega)$ and the one of the experimental available¹⁵ dynamic structure factor; the experimental single particle peak position is known to increase by about 0.8 K in moving from $q = 0.7 \text{ \AA}^{-1}$ to $q = 0.783 \text{ \AA}^{-1}$.

A. The dynamical structure factor of superfluid ^4He

Our first case study is the determination of the dynamical structure factor $S(q, \omega)$ of liquid bulk ^4He . We have used the exact SPIGS method^{20,21} to compute the intermediate scattering function $F(q, \tau)$ at $T = 0 \text{ K}$ near the equilibrium density, $\rho = 0.0218 \text{ \AA}^{-3}$, and slightly above the freezing density, $\rho = 0.0262 \text{ \AA}^{-3}$; $F(q, \tau)$ is simply $f(\tau)$ when $\hat{A} = \hat{B}^\dagger$ is chosen to be the Fourier transform of the local density operator $\hat{A} = \hat{\rho}_{\bar{q}} = \sum_{i=1}^N e^{-i\bar{q}\cdot\vec{r}_i}$. We observe that our reconstructed $S_{GIFT}(q, \omega)$ exhibits an overall structure in good agreement with experimental data: a sharp quasi-particle peak and a shallow multi-phonon maximum are present (see Fig.1). Both features appear for the first time within an analytic continuation procedure applied to a QMC study of a many-body system in the continuum. Notice that it is not appropriate to compare the widths of the two sharp quasi-particle peaks in Fig.1: in fact the experimental peak includes the broadening arising from instrumental resolution and the effect of the finite temperature; on the contrary, as explained in the following, the width of the reconstructed GIFT peak from a $T = 0$ imaginary time correlation function is only a measure of the uncertainty in reconstructing its position. In Fig.2 we show one $S_{GIFT}(q, \omega)$ in the roton region together with the excitation energies $\varepsilon(q)$ i.e., the position of the main peak as function of q . The uncertainties of $\varepsilon(q)$ correspond to the widths of the peaks σ_ε : we have checked the consistency of such identification by performing independent QMC estima-

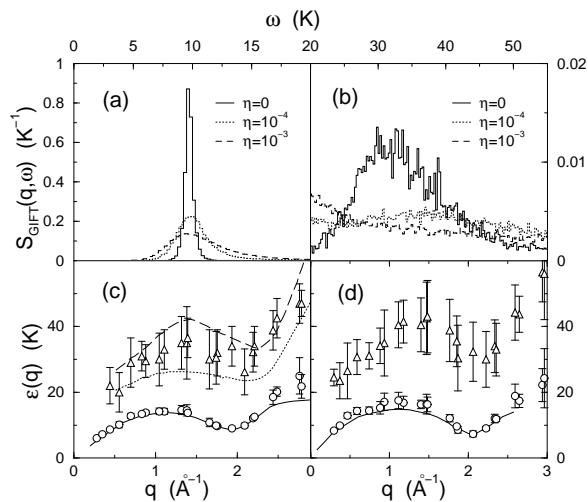


Figure 2: (a) and (b): $S_{GIFT}(q, \omega)$ at $q = 1.755 \text{ \AA}^{-1}$ and $\rho = 0.0218 \text{ \AA}^{-3}$; (a) single quasi-particle (qp) peak; (b) multiphonon (mp) contribution (notice change of scale). Lines corresponding to a $S_{GIFT}(q, \omega)$ obtained with a nonzero entropic prior ($\eta \neq 0$) are also shown. (c) $\varepsilon(q)$ extracted at $\rho = 0.0218 \text{ \AA}^{-3}$ from the position of the qp (circles) peaks and the positions of the maxima of the mp contribution (triangles) are shown. The error-bars represent the 1/2-height widths. (d) $\varepsilon(q)$ and mp contribution extracted at $\rho = 0.0262 \text{ \AA}^{-3}$. Lines in (c) and (d): experimental data^{22,23}; in the mp region in (c) the lower curve (dotted) represents the position of the maximum while the upper one (dashed) represents the 1/2-height width.

tions of $F(q, \tau)$ and comparing the positions of the peaks obtained in $S_{GIFT}(q, \omega)$; the distribution of the peaks displays a variance comparable to σ_ε^2 .

In principle also a MEM-like algorithm could fit into the GIFT approach: it is enough to modify the fitness function by adding to $\Phi_{\mathcal{D}^*}$ in equation (12) an entropic term $-\eta S$, with

$$S = \int d\omega \left\{ \bar{s}(\omega) \ln \left[\frac{\bar{s}(\omega)}{m(\omega)} \right] - \bar{s}(\omega) + m(\omega) \right\}, \quad (14)$$

S being the entropy as in Ref.6 and $\eta \geq 0$ a free parameter; $m(\omega)$ is the default model which in previous implementations^{6,7} has been chosen to be simply a constant in absence of any prior knowledge. This is not a faithful implementation of MEM because the entropic term is used in the context of the GIFT method and not within the framework of Bayes' theorem. Anyway, as we shall show, it provides results for the dynamical structure factor of superfluid ^4He very similar to the one appeared in literature.^{6,7} The tests we are going to present in the following, in our opinion strongly suggest that the entropic term makes us loose a great deal of information, enforcing the smoothness of the spectral function as already pointed out in Ref.9. A good default model could improve these results, but such *a priori* knowledge generally is not available. By using a constant as default

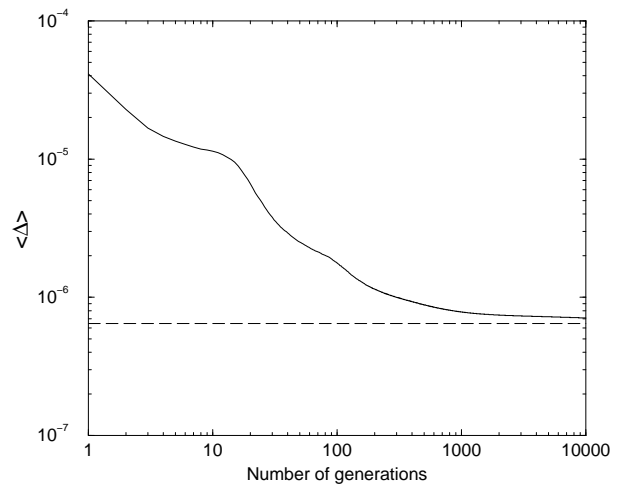


Figure 3: Evolution of the deviation (10) during the stochastic evolution of the genetic algorithm for the reconstruction plotted in Fig.2(a,b) for $\eta = 0$ averaged with respect to the sampled sets \mathcal{D}^* . The dashed horizontal line represents the value $\delta = \frac{1}{l+1} \sum_{j=0}^l \sigma_{f_j}^2$.

model, $m(\omega)$, as in previous works^{6,7}, for all wave vectors \vec{q} we observed for the main peak of $S(q, \omega)$ a broadening (see Fig.2) strongly dependent on the choice of the parameter η . This implementation of MEM provides results comparable with those reported in references 6 and 7. The overall double-peak structure is typically lost in presence of the entropic term: no sharp peak is present but only a smooth $S(q, \omega)$ survives, as function of ω , making the extracted excitation energy critically dependent on the value of η , thus introducing ambiguities in the interpretation of the results. In our original approach, i.e. without $\eta S(\bar{s})$, we have checked that none of the parameters (like \mathcal{M} , $\Delta\omega$, α , γ_n , ...) affects the class of features that we may trust to carry reliable physical information.

As an example of the stochastic evolution, in Fig.3 we show the deviation (10) as a function of the number of generations in the evolutionary process for the reconstruction plotted in Fig.2(a,b) for $\eta = 0$ averaged on the sampled sets \mathcal{D}^* . One can see that the maximum number of generations, \mathcal{N}_G , we have used in this reconstruction is optimal in reaching the “compatibility” condition, $\Delta(\bar{s}) \simeq \delta = \frac{1}{l+1} \sum_{j=0}^l \sigma_{f_j}^2$, without overfitting.

By integrating $S_{GIFT}(q, \omega)$ we have access to quantities like the strength of the single quasi-particle peak, $Z(q)$, and thus also to the contribution to the static structure factor, $S(q)$, coming from multiphonon excitations. Remarkably, $Z(q)$ turns out to be in close agreement with experimental data (see upper Fig.4), thus strongly suggesting that the shallow maximum in $S_{GIFT}(q, \omega)$ at large energy carries indeed reliable physical information on the multiphonon branch of the spectrum. The position of such multiphonon maximum (see Fig.2c) is in qualitative agreement with experiments²²: as we show in the next section, within the present implementation of

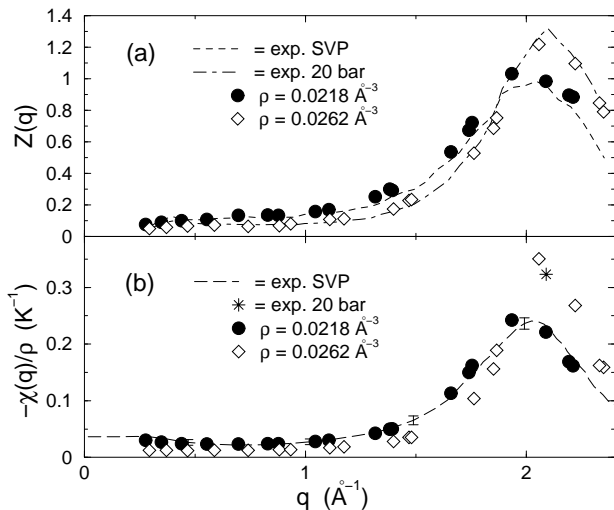


Figure 4: (a) GIFT strength of the quasi particle peak $Z(q)$ as function of q at two densities and experimental data²⁴. (b) GIFT Static density response function $\chi(q)$ at two densities and experimental data^{22,25}. Error bars of theoretical results are smaller than the symbol size.

the GIFT method there is no possibility to recover the detailed shape of the spectral function like the multiphonon substructures given by high resolution measurements²⁴ of $S(q, \omega)$. In the lower panel of Fig.4 we show the static density response function $\chi(q)$ obtained evaluating the c_{-1} from $S_{GIFT}(q, \omega)$; the agreement with experiments is impressive, also near freezing²⁵.

The calculation of the excitation spectrum $\varepsilon(q)$ in superfluid ^4He via QMC was addressed for instance in Ref.26 and in Ref.27, but here we are clearly much more ambitious because we aim to reconstruct the full spectral function. Our method is so powerful that it is able to reveal the effects of even fine details of the interatomic interaction. For example, the computed spectrum $\varepsilon(q)$ in the phonon region is about 0.7 K above the experimental value. We understand this as an effect of truncation of the inter-atomic interaction $v(r)$ at a certain distance r_c . In most of our computations the interatomic potential is cut-off and displaced to zero at $r_c = 6 \text{ \AA}$, and the equation of state gives rise to an overestimation of the sound velocity by about 16%. We have performed some computations with $r_c = 14 \text{ \AA}$, in a simulation of $N = 512$ ^4He atoms and in this case the sound velocity turns out to be correct and now the theoretical $\varepsilon(q)$ at small q agrees with experiment within the resolution $\Delta\omega$. By computing $\varepsilon(q)$ for many wave vectors in the roton region and averaging among the excitation energies nearby the roton minimum, at $\rho = 0.0218 \text{ \AA}^{-3}$ we extract a roton energy of $E_R = 8.96 \pm 0.47 \text{ K}$ with the $v(r)$ in Ref.17 and of $E_R = 8.67 \pm 0.29 \text{ K}$ with the $v(r)$ in Ref.18, a potential considered more accurate (Experimental roton energy²⁸ at SVP $E_R = 8.608 \pm 0.01 \text{ K}$). At $\rho = 0.0262 \text{ \AA}^{-3}$ we extract a roton energy of $E_R = 7.43 \pm 0.34 \text{ K}$ with the $v(r)$ in Ref.17 and of $E_R = 7.22 \pm 0.27 \text{ K}$ with

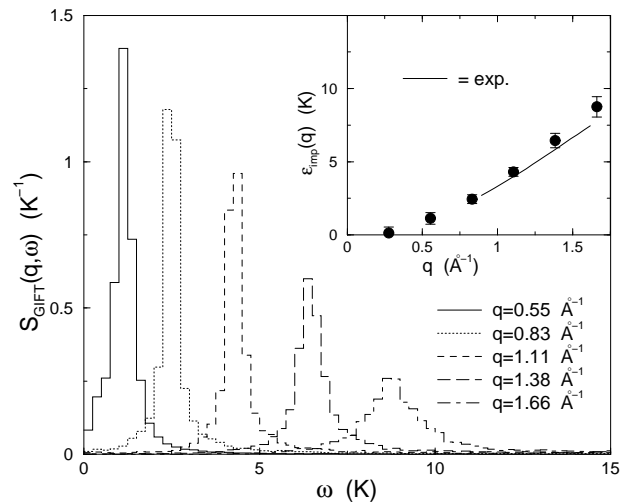


Figure 5: Impurity ^3He quasi-particle peak in superfluid ^4He at SVP for several wave vectors; in the inset the extracted excitation energies are shown together with experimental data²⁹.

the $v(r)$ in Ref.18 (Experimental roton energy²⁸ at 24 bar $E_R = 7.3 \pm 0.02 \text{ K}$).

B. Impurity and vacancy dynamics

Another interesting test case is provided by liquid ^4He in presence of one ^3He impurity, in order to extract the impurity branch which has been experimentally measured²⁹. Variational results for such branch are known³⁰ but no results from exact QMC are available. This calculation requires the choice of $\hat{A} = e^{-i\vec{q}\cdot\vec{r}_{imp}}$, where \vec{r}_{imp} is the position of the impurity. In Fig.5 we show the reconstructed spectral functions together with the estimated dispersion relation obtained from a simulation of $N = 255$ ^4He atoms and one ^3He atom at $\rho = 0.0218 \text{ \AA}^{-3}$. The agreement with experimental data²⁹ is very good, thus providing a robust check of validity of our approach.

As a further application of GIFT we have studied the excitation spectrum of a single vacancy in hcp solid ^4He at $\rho = 0.0293 \text{ \AA}^{-3}$, a density slightly above melting. The behavior of vacancies in solid ^4He is of high interest because vacancies and other defects are believed to have a key role in the possible supersolid phase of ^4He at low temperature^{31,32}. In order to apply GIFT to vacancy dynamics the first step is the definition of a vector position \vec{x}_v that allows to follow the “motion” of the vacancy in imaginary time during a SPIGS simulation. This problem is much more difficult than the evaluation of the impurity branch, because the very definition of \vec{x}_v is far from trivial due to the large zero-point motion of the atoms in the low density solid. \vec{x}_v turns out to be a many-body variable, depending on all the vector positions of ^4He atoms, and even not free of ambiguities. We

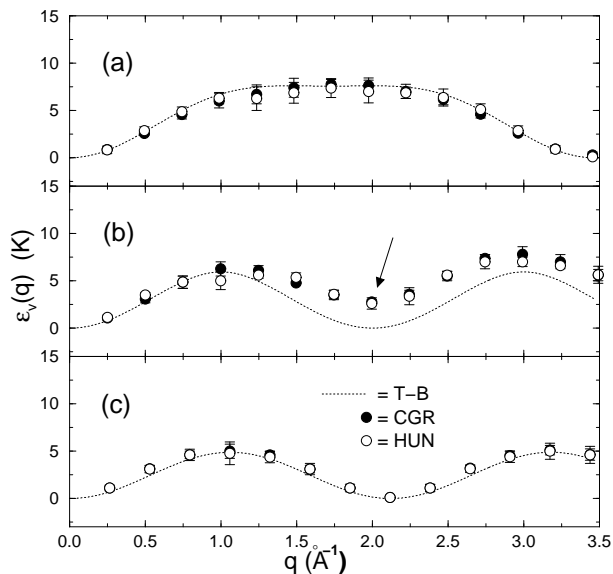


Figure 6: Vacancy excitation spectrum in solid ${}^4\text{He}$ extracted from the $S_{GIFT}(q, \omega)$ of the vacancy-vector position \vec{x}_v at $\rho = 0.0293 \text{ \AA}^{-3}$ in a hcp lattice with $N=447$ particles along the principal symmetry directions: (a) ΓK , (b) ΓM and (c) ΓA . Two different algorithms have been used to obtain \vec{x}_v : a coarse-grain algorithm³³ (CGR) and the Hungarian algorithm^{34,35} (HUN). Dotted lines represent the spectrum of a tight binding model (T-B) for the hcp lattice³⁶ obtained imposing the values of the band width along the ΓK and ΓA directions equal to the average between the values extracted from the two different algorithms. The arrow points out the vacancy-roton mode.

have employed two different procedures to obtain \vec{x}_v : the coarse-grain³³ and the Hungarian^{34,35}. In Fig.6 we show the vacancy excitation spectrum $\varepsilon_v(\vec{q})$ extracted from the vacancy spectral functions ($\hat{A} = e^{-i\vec{q}\cdot\vec{x}_v}$) obtained with the two methods. The results obtained with the two definitions of \vec{x}_v are very similar, and at first sight make evident a picture of Bloch waves in the crystal; the agreement with a tight binding hopping model³⁶ is good. Notice that $\varepsilon_v(\vec{q})$ represents the excitation energy with respect to the state with a vacancy with $|\vec{q}| = 0$, i.e., $\varepsilon_v(\vec{q})$ does not include the vacancy activation energy. By fitting $\varepsilon_v(\vec{q})$ with the tight binding expression we extract the vacancy effective mass in the different lattice directions: $m_{\Gamma K}^* = m_{\Gamma M}^* = 0.46 \pm 0.03m_4$ and $m_{\Gamma A}^* = 0.55 \pm 0.1m_4$, where m_4 is the ${}^4\text{He}$ mass; these values for m^* are in agreement with the results obtained with a different method in Ref.37.

The agreement of $\varepsilon_v(\vec{q})$ with the tight binding model fails dramatically in the ΓM direction. In fact, at any reciprocal lattice vector the excitation energy should vanish. On the contrary at the first reciprocal lattice vector along ΓM the vacancy excitation spectrum does not vanish but it reveals a novel vacancy-roton mode with an energy of $2.6 \pm 0.4 \text{ K}$ and an effective mass of about $m_R^* = 0.46 m_4$. We have checked that this energy does

not depend on the size of the system. Such behavior of $\varepsilon_v(\vec{q})$ in the ΓM direction implies that the (non-zero) minimum is not a consequence of the lattice periodicity but it is related to correlated motion of particles like in superfluid ${}^4\text{He}$. It is interesting that neutron scattering from hcp ${}^4\text{He}$ gives an unexpected excitation mode beyond the phonon modes exactly in the ΓM direction with a roton-like mode at the reciprocal wave vector³⁸. The experimental energy of such roton mode is about 4.4 times larger than what we find; so it is unclear the connection between our mode and experimental data. A larger vacancy roton energy might arise in presence of clusters of vacancies. By analyzing the contributions to $f(\tau) = \langle e^{\hat{H}\tau} \hat{A} e^{-\hat{H}\tau} \hat{A}^\dagger \rangle$ with $\hat{A} = e^{-i\vec{q}\cdot\vec{x}_v}$, one can see that the vacancy-roton mode is connected to motions of the vacancy between different basal planes. The fundamental difference between in-basal-plane and inter-basal-plane motions is that the lattice position in the first case is a centre of inversion whereas this is not so in the second case. The fact that hcp is not a Bravais lattice is fundamental in this respect. We have verified that in bcc crystal and in a two dimensional triangular lattice, both Bravais lattices, no such vacancy roton mode is present.

IV. TESTS ON KNOWN SPECTRAL MODELS

In this section we show several tests of application of the GIFT method on known analytical spectral models suitably discretized and “dirtied” with random noise to “simulate” actual data. It will appear evident what we have already pointed out in the introduction: only some features of the exact solution can be consistently reproduced; we have no possibility to reconstruct exactly the shape of $s(\omega)$; on the other hand, access is granted to the identification of the presence of peaks and to their positions, to some integral properties involving $s(\omega)$ and to its support.

The most natural test for the reliability of the GIFT approach we have developed is provided by a systematic study of Laplace inversion problems whose analytical solution is known. Our idea is to focus our attention on model functions of the form:

$$s(\omega) = \theta(\omega) \sum_{j=1}^{\mathcal{N}_p} p_j \frac{e^{-\frac{(\omega-\mu_j)^2}{2\alpha_j^2}}}{\sqrt{2\pi}\alpha_j} \quad \sum_{j=1}^{\mathcal{N}_p} p_j = 1 \quad (15)$$

linear combinations of Gaussians multiplied by $\theta(\omega)$, the Heaviside distribution, resembling qualitatively the experimental results for spectral functions in condensed matter physics at $T = 0$. We may perform several tests varying the parameters \mathcal{N}_p , number of maxima, $\{\mu_1, \dots, \mu_{\mathcal{N}_p}\}$, positions of the maxima, $\{\alpha_1, \dots, \alpha_{\mathcal{N}_p}\}$, widths of the peaks and $\{p_1, \dots, p_{\mathcal{N}_p}\}$, the areas under the peaks. The Laplace transform $f(\tau)$ of (15) may be expressed in terms of the standard complementary error

function:

$$\operatorname{erfc}(z) = \frac{2}{\sqrt{\pi}} \int_z^{+\infty} dt e^{-t^2}, \quad (16)$$

whose values are tabulated, in the following form:

$$f(\tau) = \frac{1}{2} \sum_{j=1}^{\mathcal{N}_p} p_j e^{-\mu_j \tau + \frac{\tau^2 \alpha_j^2}{2}} \operatorname{erfc} \left(\frac{\tau \alpha_j - \mu_j / \alpha_j}{\sqrt{2}} \right) \quad (17)$$

In order to *simulate* the output of a typical QMC calculation, we define the *measured imaginary time data* $\mathcal{F} = \{f_0, \dots, f_l\}$ as:

$$f_j = f(j\delta\tau) + \varepsilon_j \quad (18)$$

where $f(j\delta\tau)$ is evaluated from (17), and ε_j are random numbers, mimicking the error bars affecting QMC data, following Gaussian distributions with zero mean and variances, $\sigma_{\varepsilon_j}^2$, comparable with the ones typically occurring in our QMC results ($\sigma_{\varepsilon_j}/f_j$ in the range 0.1–4 %). f_j play the role of the output of QMC simulation; GIFT falsification uses \mathcal{N}_r random sets $\mathcal{F}^* = \{f_0^*, \dots, f_l^*\}$ defined by

$$f_j^* = f_j + \varepsilon_j^* \quad (19)$$

ε_j^* being Gaussian random variables with zero mean and variances which here, to be coherent with the applications we have presented, we assume to be equal to $\sigma_{\varepsilon_j}^2$.

Our aim is to compare (15) with the GIFT result we obtain pretending that our knowledge about the imaginary time correlation function is limited to the discretized and noisy data \mathcal{F} in (18), and to other available information about the moments c_n which, inside these tests on analytically solvable models, can be evaluated from (15); we will neglect now the error bars affecting the values of the c_n . The parameters we have employed in our GIFT reconstructions are listed in Table I. Obviously, the choices of the interval of the frequency space, of the resolution $\Delta\omega$ (which fixes N_ω), of the discretization $\Delta\tau$ and of the number of points in imaginary time l are crucial for a specific spectral function one is trying to reconstruct and should be chosen consistently with the considered model; the other parameters are not crucial for a correct functioning of the GIFT method and they have been chosen in order to falsify a wide variety of models leaving the computational cost of the algorithm at a reasonable level.

Also in the reconstruction of known models of spectral functions one can compare GIFT results with those based on the strategy of MEM by adding in the fitness function an entropic term, as we did with the dynamical structure factors in superfluid ^4He from QMC imaginary time correlation functions.

A. Single peak reconstruction

The simplest test-case is provided by the attempt of reconstructing spectral functions displaying only one peak

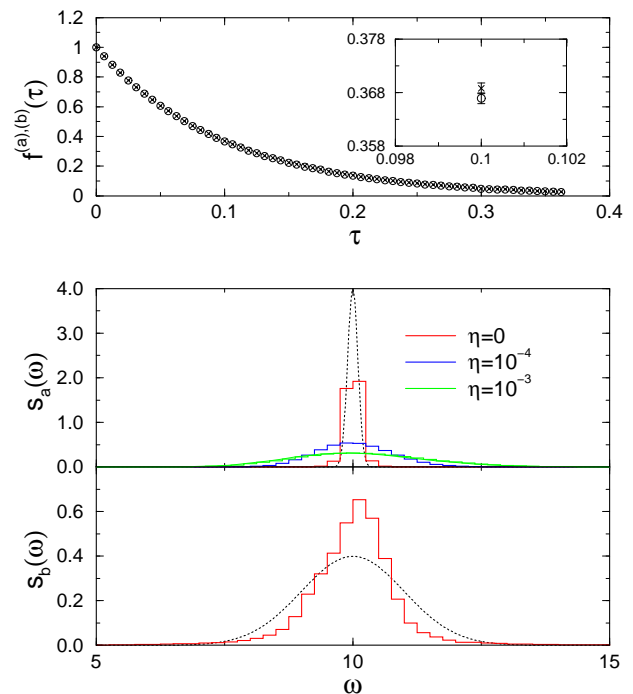


Figure 7: (Color online) Single peak reconstruction. Upper panel: Two noisy imaginary time correlation functions obtained via (18) from $f^{(a)}(\tau)$ (open circles) and $f^{(b)}(\tau)$ (x symbols), which are the Laplace transforms of $s_a(\omega)$ (dotted line in the middle panel: $\mu = 10$ and $\alpha = 0.1$) and $s_b(\omega)$ (dotted line in the lower panel: $\mu = 10$ and $\alpha = 1$). The inset is a zoom on one imaginary time instant. Middle panel: $s_a(\omega)$ (dotted line) and reconstructed $S_{GIFT}(\omega)$ (red line) using in the fitness $\Phi_{\mathcal{D}^*}$ only the first moment c_1 (i.e. $\gamma_n = 0 \forall n \neq 1$); green and blue lines represent MEM-like reconstructions with different values of the η parameter in the fitness (see legend). Lower panel: $s_b(\omega)$ (dotted line) and reconstructed $S_{GIFT}(\omega)$ using in the fitness $\Phi_{\mathcal{D}^*}$ only the first moment c_1 (i.e. $\gamma_n = 0 \forall n \neq 1$).

at a given point μ with a width α . The upper panel of Fig. 7 makes evident the difficulty of the inverse problem: two functions with the same parameter $\mu_a = \mu_b = 10$ but different values of the widths, respectively $\alpha_a = 0.1$ and $\alpha_b = 1.0$, in imaginary time domain differ by about 0.5%, of the same order as the typical QMC error bars. It is clear then that the information about the width of the peak is always strongly obscured by the noise. However, from the middle and lower panel of Fig. 7 it is manifest that GIFT reconstruction, obtained using in the fitness $\Phi_{\mathcal{D}^*}$ only the first moment c_1 (i.e. $\gamma_n = 0 \forall n \neq 1$), is able to capture with an high accuracy the position of the peak in both cases. We note that, despite the difficulty mentioned above, in this simple case of a single peak, even the widths are remarkably semi-quantitatively recovered. This ability is evidently lost when the entropic term with a constant default model is switched on (see Fig.7).

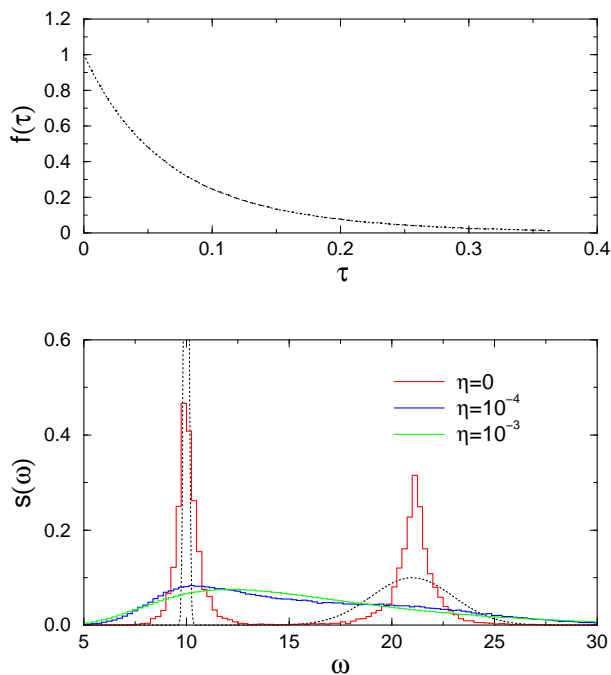


Figure 8: (Color online) Double peak reconstruction for well separated peaks. Upper panel: Noisy imaginary time correlation function obtained via (18) from $f(\tau)$ (dotted line) which is the Laplace transform of $s(\omega)$ (dotted line in the lower panel, see text for parameters). Lower panel: $s(\omega)$ (dotted line) and reconstructed $S_{GIFT}(\omega)$ (red line) from $f(\tau)$ using in the fitness $\Phi_{\mathcal{D}^*}$ only the first moment c_1 (i.e. $\gamma_n = 0 \forall n \neq 1$); green and blue lines represent MEM-like reconstructions with different values of the η parameter in the fitness (see legend).

	name of the parameter	symbol	value
SM	number of bins in frequency space	N_ω	600
SM	resolution in frequency space	$\Delta\omega$	0.25
SM	number of quanta of spectral weight	\mathcal{M}	5×10^3
CF	discretization in imaginary time	$\delta\tau$	1/160
CF	number of points in imaginary time	l	60
GA	number of generations	$\mathcal{N}_{\mathcal{G}}$	10^4
GA	initial number of models	$\mathcal{N}_{\overline{s}}$	2.5×10^4
GA	final number of models	$\mathcal{N}_{\overline{s}}$	400
GA	number of new random sets generated	\mathcal{N}_r	10^3

Table I: Typical parameters used with the GIFT method related to: the space of models (SM), the correlation function (CF) and the genetic algorithm (GA).

B. Double peak reconstruction

In order to get closer to realistic physical applications, we try to reconstruct also spectral functions displaying a double peak. Inside such a double peak reconstruction, we may check also the estimation of the integrated

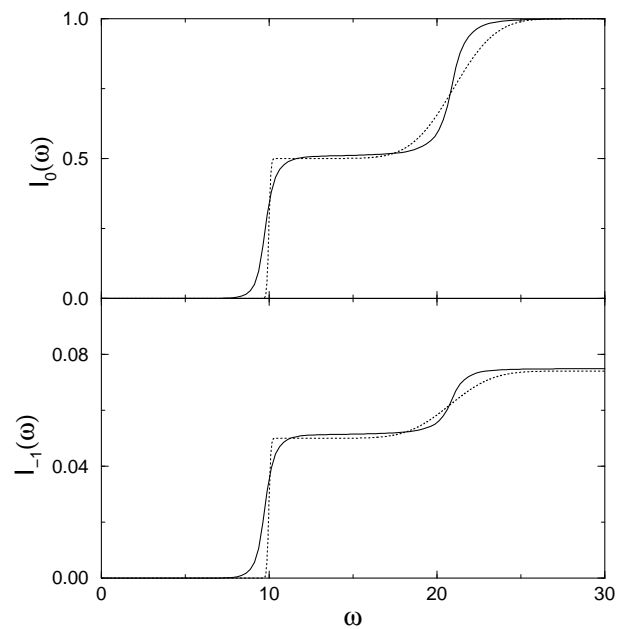


Figure 9: Integral properties for double peak reconstruction. Upper panel: $I_0(\omega)$ from the exact $s(\omega)$ (dotted line) and $I_0(\omega)$ obtained with the reconstructed $S_{GIFT}(\omega)$ in Fig. 8 (case $\eta = 0$). Lower panel: $I_{-1}(\omega)$ from the exact $s(\omega)$ (dotted line) and $I_{-1}(\omega)$ obtained with the reconstructed $S_{GIFT}(\omega)$ in Fig. 8.

spectral functions:

$$\begin{aligned}
 I_0(\omega) &= \int_0^\omega d\omega' s(\omega') \quad , \\
 I_{-1}(\omega) &= \int_0^\omega d\omega' \frac{s(\omega')}{\omega'} \quad .
 \end{aligned}
 \tag{20}$$

$I_0(\omega)$ provides information about the spectral weight under the peaks in $s(\omega)$; in particular in the ω range between the two peaks $I_0(\omega)$ gives the information from which we have derived the strength of the single quasi-particle peak, $Z(q)$, in our GIFT study of superfluid ${}^4\text{He}$, as we will show in the following section. On the other hand, the asymptotic value of $I_{-1}(\omega)$ for large ω provides the key to estimate the static response function $\chi(q)$.

In Fig. 8 we show a reconstruction of a spectral function $s(\omega)$ for two well separated peaks ($p_1 = 0.5, p_2 = 0.5, \mu_1 = 10, \mu_2 = 21, \alpha_1 = 0.1$ and $\alpha_2 = 2.0$) using in the fitness $\Phi_{\mathcal{D}^*}$ only the first moment c_1 (i.e. $\gamma_n = 0 \forall n \neq 1$); this is the typical fitness used in our reconstruction of spectral functions of superfluid ${}^4\text{He}$. The corresponding $I_0(\omega)$ and $I_{-1}(\omega)$ are plotted in Fig. 9 compared with the analytic results from (15). We observe that no appreciable difference emerges, with respect to the exact results, as far as the determination of the positions of the peaks, of the areas under the peaks, and of the c_{-1} moment (see Fig. 9) are concerned: the accuracy is very good; on the other hand, the shape of the reconstructed $s(\omega)$ has not to be taken too seriously because it be-

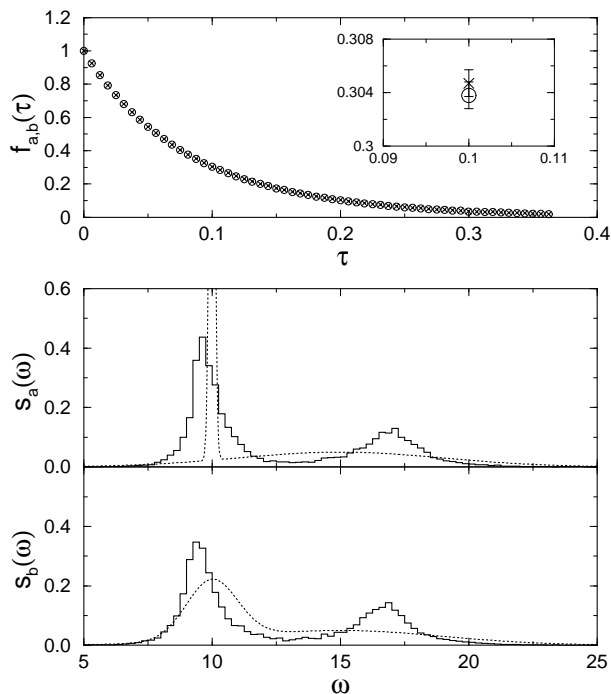


Figure 10: Double peak reconstruction for overlapping peaks. Upper panel: Two noisy imaginary time correlation functions obtained via (18) from $f^{(a)}(\tau)$ (open circles) and $f^{(b)}(\tau)$ (x symbols), which are the Laplace transforms of $s_a(\omega)$ (dotted line in the middle panel) and $s_b(\omega)$ (dotted line in the lower panel); see text for parameters. The inset is a zoom on one imaginary time instant. Middle panel: $s_a(\omega)$ (dotted line) and reconstructed $S_{GIFT}(\omega)$ using in the fitness $\Phi_{\mathcal{D}^*}$ only the first moment c_1 (i.e. $\gamma_n = 0 \forall n \neq 1$). Lower panel: $s_b(\omega)$ (dotted line) and reconstructed $S_{GIFT}(\omega)$ using in the fitness $\Phi_{\mathcal{D}^*}$ only the first moment c_1 (i.e. $\gamma_n = 0 \forall n \neq 1$).

longs to the class of properties whose determination is obscured by statistical errors and discretization in imaginary time. MEM-like reconstructions are not even able to detect the presence of two peaks; moreover the position of the maximum of the reconstructed spectral function is dangerously η -dependent (see Fig. 8).

In Fig. 10 we consider two different spectral functions $s_a(\omega)$ and $s_b(\omega)$, characterized by two overlapping peaks, whose Laplace transforms, in imaginary time domain, are plotted in the upper panel ($p_{1a} = 0.5$, $p_{2a} = 0.5$, $\mu_{1a} = 10$, $\mu_{2a} = 15$, $\alpha_{1a} = 0.1$ and $\alpha_{2a} = 4.0$; $p_{1b} = 0.5$, $p_{2b} = 0.5$, $\mu_{1b} = 10$, $\mu_{2b} = 15$, $\alpha_{1b} = 1.0$ and $\alpha_{2b} = 4.0$) As discussed previously, the small difference, comparable with the (pretended) error bars, rules out the possibility of a reconstruction of the actual shapes. Nevertheless, the GIFT method succeeds in finding out the positions of the peaks with good accuracy even in this case in which the overlap between the two peaks becomes significant.

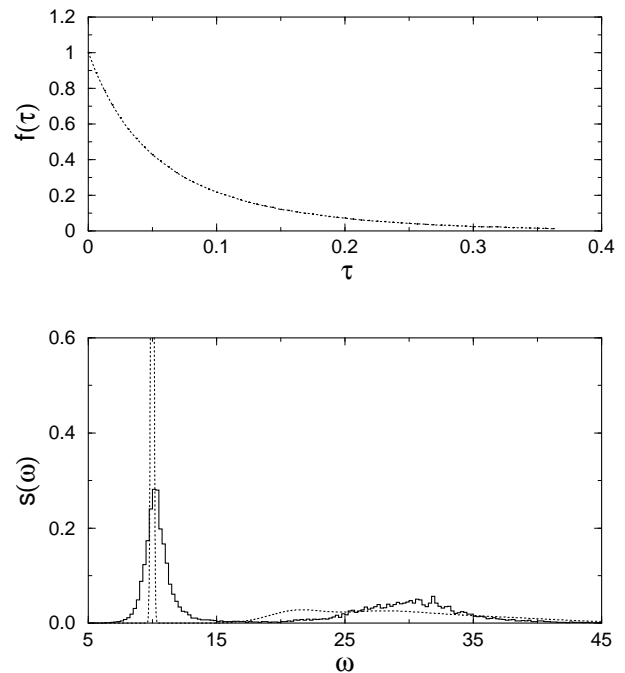


Figure 11: Multiple peak reconstruction. Upper panel: Noisy imaginary time correlation function obtained via (18) from $f(\tau)$ which is the Laplace transform of $s(\omega)$ (dotted line in the lower panel). Lower panel: $s(\omega)$ (dotted line) and reconstructed $S_{GIFT}(\omega)$ from $f(\tau)$ using in the fitness $\Phi_{\mathcal{D}^*}$ only the first moment c_1 (i.e. $\gamma_n = 0 \forall n \neq 1$).

C. Multiple peak reconstruction

Finally, we devise the following test: we try to reconstruct a spectral function $s(\omega)$ ($p_1 = 0.5$, $p_2 = 0.1$, $p_3 = 0.2$, $p_4 = 0.2$, $\mu_1 = 10$, $\mu_2 = 21$, $\mu_3 = 27$, $\mu_4 = 35$, $\alpha_1 = 0.1$, $\alpha_2 = 2$, $\alpha_3 = 4$, $\alpha_4 = 6$), displaying a main peak and a broad contribution at higher ω , made of a superposition of three Gaussians, resembling qualitatively the *shape* of the multiphononic contribution in the dynamical structure factor of superfluid ^4He . We have tested our method using the usual fitness function $\Phi_{\mathcal{D}^*}$ with only the first moment c_1 included (i.e. $\gamma_n = 0 \forall n \neq 1$): the results are plotted in Fig. 11. In Fig. 12 the integrated spectral functions are plotted; from the comparison between the exact $I_0(\omega)$ and the one obtained from the reconstructed $S_{GIFT}(\omega)$ one can observe that the spectral weights under the main peak and the broad contribution are well reproduced. Also the large ω limit of $I_{-1}(\omega)$ is in good agreement with the exact value.

One can also study the effect of the noise in $f(\tau)$ in order to check the GIFT ability in recovering correct information on the true $s(\omega)$. In Fig. 13 we show two $S_{GIFT}(\omega)$ reconstructed from a noisy $f(\tau)$ with σ_{ε_j} 10 times and 50 times greater than in the test shown in Fig. 11. Only in the second case, which represents a situation of very high relative noise ($\sigma_{\varepsilon_j}/f_j$ in the range 5–200 %), information on the correct spectral function is sensi-

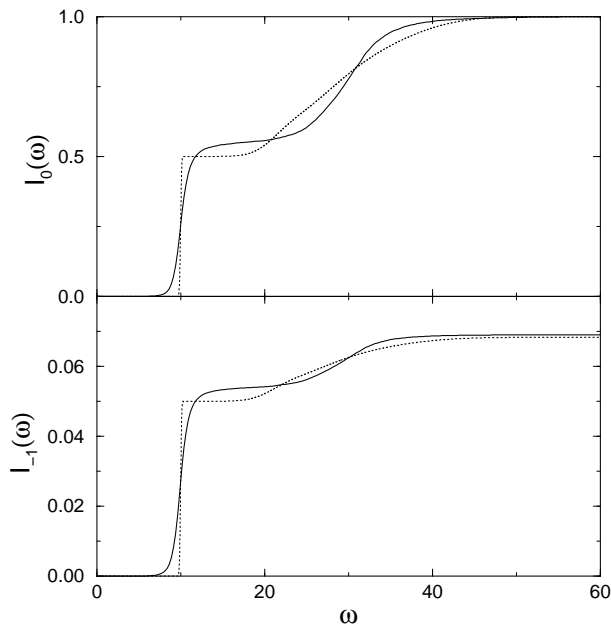


Figure 12: Integral properties for multiple peak reconstruction. Upper panel: $I_0(\omega)$ from the exact (dotted line) and $I_0(\omega)$ obtained with the reconstructed $S_{GIFT}(\omega)$ in Fig. 11. Lower panel: $I_{-1}(\omega)$ from the exact (dotted line) and $I_{-1}(\omega)$ obtained with the reconstructed $S_{GIFT}(\omega)$ in Fig. 11.

bly lost. This test show the robustness of GIFT against noise in the observations, being able to recover correct information on $s(\omega)$ with a noise level up to one order of magnitude greater than what can be easily obtained in typical QMC calculations of imaginary-time correlation functions.

It is possible also to use GIFT with a limited information on $f(\tau)$, which corresponds as usual to $f(\tau)$ values for a discrete set of imaginary times, but without any added noise. The result of such GIFT multi-peak reconstruction is shown in the upper panel of Fig. 14. By comparing this result with that shown in Fig. 11 it is possible to see that the two $S_{GIFT}(\omega)$ are very similar thus ruling out the necessity of more accurate observations of $f(\tau)$ at discrete imaginary times in order to improve the GIFT performance. By maintaining the noise level in f_j to zero, we have also tried to increase the amount of information by using $l = 240$ number of points in imaginary time with $\delta\tau = 1/640$; the result of such GIFT multi-peak reconstruction is shown in the middle panel of Fig. 14. No substantial improvement can be observed with respect to the previous case in spite of an increased computational cost of the GIFT algorithm. The computational cost of GIFT is increased also by considering a wider space of model spectral functions. In our last test we tried a GIFT multi-peak reconstruction without noise with $\Delta\omega = 0.1$, the number of bins in frequency space $N_\omega = 1500$ and the “quantization” of spectral weight $\mathcal{M} = 10^4$. The result is shown in the lower panel of Fig. 14; here the noise in $S_{GIFT}(\omega)$ is higher because due

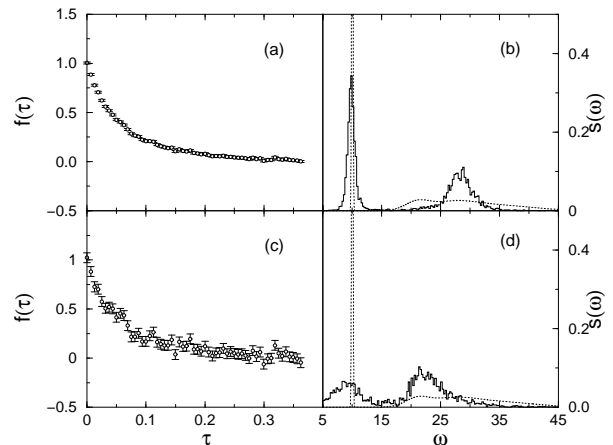


Figure 13: Panel (a): f_j values obtained with $\sigma_{\varepsilon_j} = 0.01$ and used by GIFT to reconstruct $s(\omega)$ as shown in panel (b). Panel (c): f_j values obtained with $\sigma_{\varepsilon_j} = 0.05$ and used by GIFT to reconstruct $s(\omega)$ as shown in panel (d). Panel (b): exact $s(\omega)$ (dotted line) as in Fig. 11 and reconstructed $S_{GIFT}(\omega)$ using the noisy observation of $f(\tau)$ in panel (a). Panel (d): exact $s(\omega)$ (dotted line) as in Fig. 11 and reconstructed $S_{GIFT}(\omega)$ using the noisy observation of $f(\tau)$ in panel (c).

to the computational cost of the GIFT algorithm with this parameters we have only averaged over $\mathcal{N}_r = 160$ random sets. Also in this case we found no substantial improvement in $S_{GIFT}(\omega)$ as compared to the standard case.

In the previous tests we have not explored different variants of GIFT as, for instance, a basis set different from step functions; one cannot exclude the possibility that by using different variants of this method more information could be obtained.

V. CONCLUSIONS

We have built up a new strategy to attack inverse problems which has been used to study dynamics in quantum many-body systems from QMC simulations; we have obtained very accurate results in the ^4He case, in the liquid and in the solid phase, even in presence of disorder, providing major improvements with respect to previous studies appeared in literature on this case. We have stressed the important point that the problem we have faced belongs to the huge class of inverse problems, a deep topic also from a fundamental epistemological⁴ point of view. The basic idea of the falsification principle³ guided us in our particular implementation of analytic continuation, but, of course, may provide important implications in many fields of scientific research. Moreover, every problem emerging in Physics or applied Mathematics that could be cast in the form of equation (2), independently of the specific kernel in equation (2), can be attacked with GIFT. The method can be extended to in-

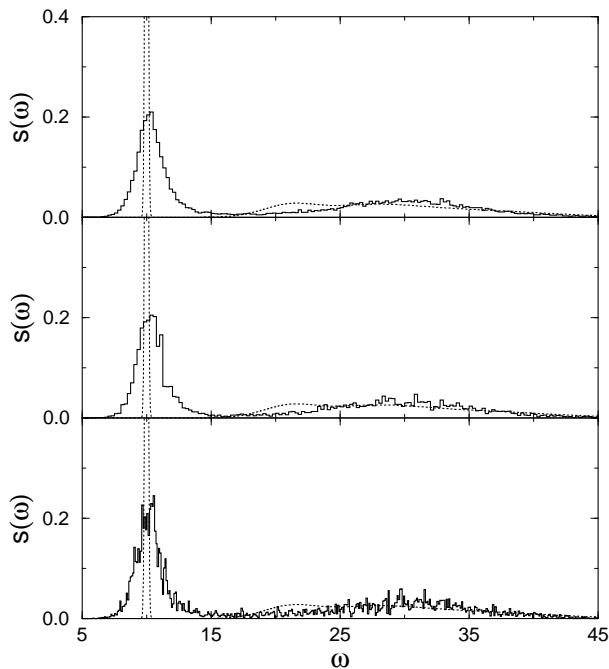


Figure 14: $s(\omega)$ (dotted line) as in Fig. 11. Upper panel: reconstructed $S_{GIFT}(\omega)$ from the exact $f(\tau)$ (i.e. without noise) assumed to be known for $l = 60$ number of points in imaginary time with $\delta\tau = 1/160$, with $\Delta\omega = 0.25$ and using in the fitness $\Phi_{\mathcal{D}^*}$ only the first moment c_1 (i.e. $\gamma_n = 0 \forall n \neq 1$). Middle panel: reconstructed $S_{GIFT}(\omega)$ from the exact $f(\tau)$ (i.e. without noise) assumed to be known for $l = 240$ number of points in imaginary time with $\delta\tau = 1/640$, with $\Delta\omega = 0.25$ and using in the fitness $\Phi_{\mathcal{D}^*}$ only the first moment c_1 (i.e. $\gamma_n = 0 \forall n \neq 1$). Lower panel: reconstructed $S_{GIFT}(\omega)$ from the exact $f(\tau)$ (i.e. without noise) assumed to be known for $l = 60$ number of points in imaginary time with $\delta\tau = 1/160$, with $\Delta\omega = 0.1$ and using in the fitness $\Phi_{\mathcal{D}^*}$ only the first moment c_1 (i.e. $\gamma_n = 0 \forall n \neq 1$).

clude different kinds of constraints on the spectral function or additional information like cross correlations between the statistical noise of $f(\tau)$ at different imaginary times. Many variants of GIFT can be devised depending on the problem, for instance a basis set different from step functions (5) can be used or non uniform discretization in presence of problems with multiple time scales, or distribution of noise that is not Gaussian.

VI. ACKNOWLEDGMENTS

We acknowledge useful discussions with S. Moroni, A. Motta and M. Nava. This work was supported by the Supercomputing facilities of CILEA.

-
- ¹ L. Pääväranta, E. and Somersalo (Eds.) *Inverse Problems in Mathematical Physics* (Springer-Verlag Berlin, Heidelberg 1993).
- ² J. Kaipio and E. Somersalo, *Statistical and Computational Inverse Problems* (Springer-Verlag, New York 2004).
- ³ A. Tarantola, *Nature Physics* **2**, 492 (2006).
- ⁴ K. Popper, *The Logic of Scientific Discovery* (Basic Books, 1959).
- ⁵ M. Jarrel, and J.E. Gubernatis, *Phys. Rep.* **269**, 133 (1996).
- ⁶ M. Boninsegni, and D.M. Ceperley, *J. Low Temp. Phys.* **104**, 339 (1996).
- ⁷ S. Baroni, and Moroni, S. *Phys. Rev. Lett.* **82**, 4745 (1999).
- ⁸ S.R. White, in *Computer Simulation Studies in Condensed Matter Physics III*, 145–153 (Springer-Verlag Berlin, Heidelberg 1991).
- ⁹ O.F. Syljuåsen, *Phys. Rev. B* **78**, 174429 (2008).
- ¹⁰ D.R. Reichman, and E. Rabani, *J. Chem. Phys.* **131**, 054502 (2009).
- ¹¹ J.E. Gentle, *Random Number Generation and Monte Carlo Methods* (Springer, 2003).
- ¹² D.E. Goldberg, *Genetic Algorithms in Search, Optimization, and Machine Learning* (Addison-Wesley, 1989).
- ¹³ E. Vitali, D.E. Galli, and L. Reatto, *Journal of Physics: Conference Series* **150**, 032116 (2009).
- ¹⁴ \mathcal{D}^* is obtained as before by sampling independent Gaussian distributions centered on the original observations \mathcal{D} , with variances which correspond to the estimated statistical uncertainties.
- ¹⁵ K.H. Andersen, W.G. Stirling, R. Scherm, A. Stunault, B. Fåk, H. Godfrin, and A.J. Dianoux, *J. Phys.: Cond. Matt.* **6**, 821 (1994).
- ¹⁶ A. Motta, *Statistical Inverse Problems: application to quantum dynamics*, Master thesis, Università degli Studi di Milano (unpublished).
- ¹⁷ R.A. Aziz, V.P.S. Nain, J.S. Carley, W.L. Taylor, G.T. and McConville, *J. Chem. Phys.* **70**, 4330 (1979).
- ¹⁸ R.A. Aziz, A.R. Janzen, M.R. Moldover, *Phys. Rev. Lett.* **74**, 1586 (1995).
- ¹⁹ D.M. Ceperley, *Rev. Mod. Phys.* **67**, 279 (1995).

- ²⁰ D.E. Galli, and L. Reatto, *Mol. Phys.* **101**, 1697 (2003).
- ²¹ D.E. Galli, and Reatto, L. *J. Low Temp. Phys.* **136**, 343 (2004).
- ²² R.A. Cowley, and A.D.B. Woods, *Can. J. Phys.* **49**, 177 (1971).
- ²³ A.D.B. Woods, and R.A. Cowley, *Rep. Prog. Phys.* **36**, 1135 (1973).
- ²⁴ M.R. Gibbs, K.H. Andersen, W.G. Stirling, and H. Schober, *J. Phys.: Condens. Matter* **11**, 603 (1999).
- ²⁵ F. Caupin, J. Boronat, and K.H. Andersen, *J. Low Temp. Phys.* **152**, 108 (2008).
- ²⁶ S. Moroni, D.E. Galli, S. Fantoni, and L. Reatto, *Phys. Rev. B* **58**, 909 (1998).
- ²⁷ J. Boronat, and J. Casulleras, *J. Low Temp. Phys.* **110**, 443 (2008).
- ²⁸ W.G. Stirling, in *Excitations in Two-Dimensional and Three-Dimensional Quantum Fluids* 25–46 (Plenum Press, New York 1991).
- ²⁹ B. Fåk, K. Guckelsberger, M. Körfer, R. Scherm, and A.J. Dianoux, *Phys. Rev. B*, **41**, 8732 (1990).
- ³⁰ D.E. Galli, G.L. Masserini, and L. Reatto, *Phys. Rev. B* **60**, 3476 (1999).
- ³¹ E. Kim, and M.H.W. Chan, *Nature* **427**, 225 (2004).
- ³² E. Kim, and M.H.W. Chan, *Science* **305**, 1941 (2004).
- ³³ N. Prokof'ev, and B. Svistunov, *Phys. Rev. Lett.* **94**, 155302 (2005).
- ³⁴ R.E. Burkard, and U. Derigs, *Assignment and Matching Problems* (Springer-Verlag, Berlin, 1980).
- ³⁵ B.K. Clark, and D.M. Ceperley, *Com. Phys. Comm* **179**, 82 (2008).
- ³⁶ D.E. Galli, and L. Reatto, *Phys. Rev. Lett.* **90**, 175301 (2003).
- ³⁷ Pollet. L, M. Boninsegni, A.B. Kuklov, N.V. Prokof'ev, B.V. Svistunov, and M. Troyer, *Phys. Rev. Lett.* **101**, 097202 (2008).
- ³⁸ E. Blackburn, J. Goodkind, S.K. Sinha, C. Broholm, J. Copley, and R. Erwin, *PRAMANA-J. Phys.* **71**, 673 (2008).